Bioconjugate Chemistry

Article

pubs.acs.org/bc

Tumor-Homing Glycol Chitosan-Based Optical/PET Dual Imaging Nanoprobe for Cancer Diagnosis

Sangmin Lee,[†] Sun-Woong Kang,[‡] Ju Hee Ryu,[†] Jin Hee Na,[†] Dong-Eun Lee,[§] Seung Jin Han,[†] Choong Mo Kang,[∥] Yearn Seong Choe,[∥] Kyo Chul Lee,[#] James F. Leary,[⊥] Kuiwon Choi,[†] Kyung-Han Lee,*[,∥] and Kwangmeyung Kim*[,†]

[†]Center for Theragnosis, Biomedical Research Institute, Korea Institute of Science and Technology (KIST), Seoul 136-791, Republic of Korea

[‡]Next-generation Pharmaceutical Research Center, Korea Institute of Toxicology, Daejeon 305-343, Republic of Korea

[§]Advanced Radiation Technology Institute, Korea Atomic Energy Research Institute, Jeonbuk 580-185, Republic of Korea

[∥]Department of Nuclear Medicine, Samsung Medical Center, Sungkyunkwan University School of Medicine, Seoul 135-710, Republic of Korea

[#]Molecular Imaging Research Center, Korea Institute of Radiological and Medical Sciences, Seoul 139-706, Republic of Korea

[⊥]Departments of Pharmaceutics and Biomedical Engineering, Purdue University, West Lafayette, Indiana 47907, United States

Supporting Information

ABSTRACT: Imaging techniques including computed tomography, magnetic resonance imaging, and positron emission tomography (PET) offer many potential benefits to diagnosis and treatment of cancers. Each method has its own strong and weak points. Therefore, multimodal imaging techniques have been highlighted as an alternative method for overcoming the limitations of each respective imaging method. In this study, we fabricated PET/optical activatable imaging probe based on glycol chitosan nanoparticles (CNPs) for multimodal imaging. To prepare the dual PET/optical probes based on CNPs, both ^{64}Cu radiolabeled DOTA complex and activatable matrix metalloproteinase (MMP)-sensitive peptide were chemically conjugated onto azide-functionalized CNPs via bio-orthogonal click chemistry, which was a reaction between azide group and dibenzyl cyclooctyne. The PET/optical activatable imaging probes were visualized by PET and optical imaging system. Biodistribution of probes and activity of MMP were successfully measured in tumor-bearing mice.

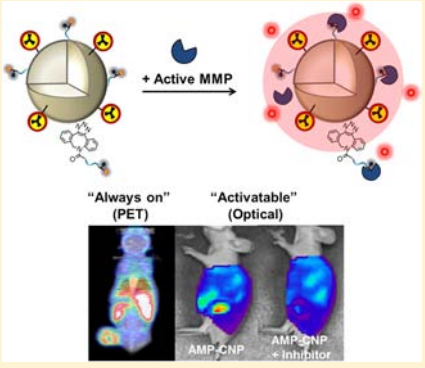

INTRODUCTION

Accurate diagnosis of cancer information is absolutely essential to select optimal treatment planning. Indeed, numerous approaches have been developed to find cancer in human body.[1−4] In particular, imaging techniques using computed tomography (CT), magnetic resonance imaging (MRI), and single-photon emission computed tomography (SPECT) play a critical role in improving diagnosis of cancer.[5−9] These imaging techniques provide convenience and sufficient anatomical information with high spatial resolution.[7,8] Although these imaging techniques can readily discover cancer in human body, diagnosis of cancer using CT, MRI, and SPECT have the limitation of insufficient information about the underlying metabolic and molecular aberrations.

One of the major thrusts in diagnosis of cancer is to provide biological characteristics that could select optimal treatment because any particular treatment provides effectiveness in some patients but ineffectiveness in others.[10] Indeed, some biological marker could provide a key for development of an anticancer drug which blocks the progression of cancer.[11−13] Positron emission tomography (PET) is an excellent technique for diagnosing and determining the stages of many types of cancers, including lung, colorectal, breast, pancreatic, and brain cancers using different tissue metabolic activity by virtue of the regional glucose uptake.[14−16] In addition, PET can provide longitudinal imaging with excellent sensitivity and yields quantitative information from whole body PET images.[17,18] However, PET has limitations in detecting specific molecular targets such as protease activity. In contrast, optical imaging can provide functional details about expression and activity of specific molecules using near-infrared fluorescence (NIRF) optical probe. Therefore, the combination of these two imaging modalities overcomes each weakness and enhances strengths.

In particular, for effective multimodal cancer imaging, it is critical for imaging probes to be complementarily tailored by biocompatible nanoparticles. The nanoparticles can be

Received: January 14, 2014
Revised: February 7, 2014
Published: February 7, 2014

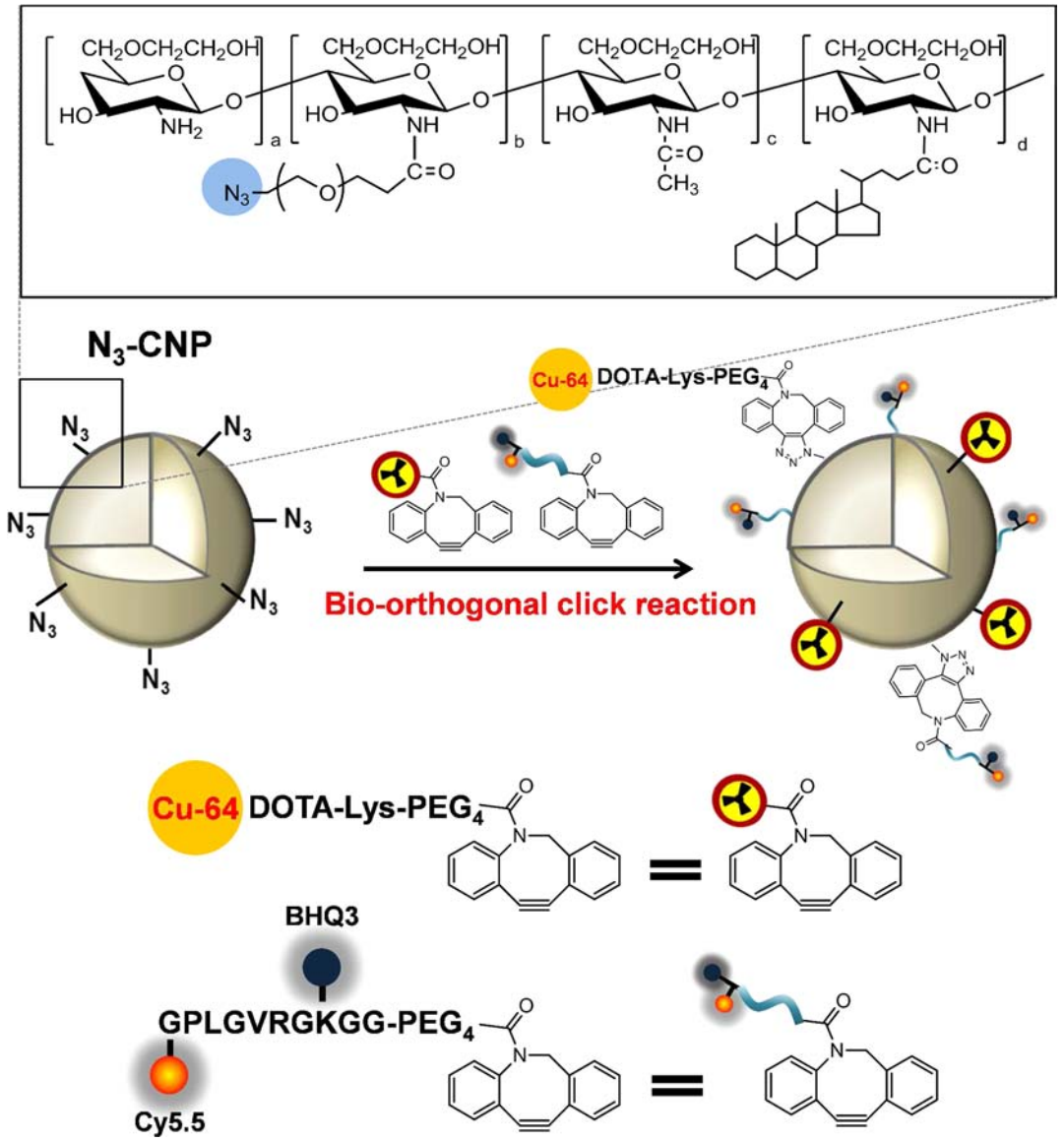

Figure 1. Chemical structure of azide-functionalized glycol chitosan-5β-cholanic acid conjugate (CNP-N_3) and schematic illustration for the labeling of DOTA-Lys-PEG_4-DBCO with ^{64}Cu and AMP-DBCO (AMP-DBCO is composed of MMP-specific peptide, NIRF dye (Cy5.5), dark quencher (BHQ-3), and DBCO) onto azide-functionalized CNP via bio-orthogonal click chemistry.

functionalized with specific targeting agent and various imaging probes to improve the specificity and sensitivity of diagnostic imaging.[19−21] In addition, nanoparticles exhibit excellent EPR effect in tumor tissues.[22,23] We already developed protease activatable probe strategies consisting internally of an activatable dark-quenched fluorogenic peptide Cy5.5−peptide substrate. These probes were successfully used as an efficient activatable optical contrast agent to image various protease-associated diseases in vivo.[24−27] Recently, we developed radiolabeled glycol chitosan nanoparticles (CNPs) as a probe for PET imaging using efficient bio-orthogonal click chemistry.[28] The introduction of bio-orthogonal click chemistry for radiolabeling to nanoparticles has accelerated preparation of imaging agent for PET imaging. However, although considerable improvement has been made in the design and synthesis of imaging probes, those studies were not focused on the development of PET/optical activatable imaging probe based on glycol chitosan nanoparticles.

Herein, the purpose of this study was to investigate PET/optical activatable imaging agents into a single nanoparticle system. Herein, both radionuclide ^{64}Cu ($T_{1/2}$ of 12.7 h) and activatable matrix metalloproteinase (MMP)-specific peptide probe were chemically conjugated into CNPs via bio-orthogonal click chemistry. A physicochemical property of PET/optical activatable imaging agents was performed using size distribution analysis and TEM image. In addition, the PET/optical activatable imaging probes were visualized by PET and optical imaging system. Biodistribution of probes and activity of MMP were successfully measured in tumor-bearing mice by PET and optical imaging system, respectively. We selected MMPs as a target of optical activatable imaging for this study because MMPs that were overexpressed in tumor sites are known to play critical roles in tumor progression and metastasis.[29,30]

dx.doi.org/10.1021/bc500020g | *Bioconjugate Chem.* 2014, 25, 601−610

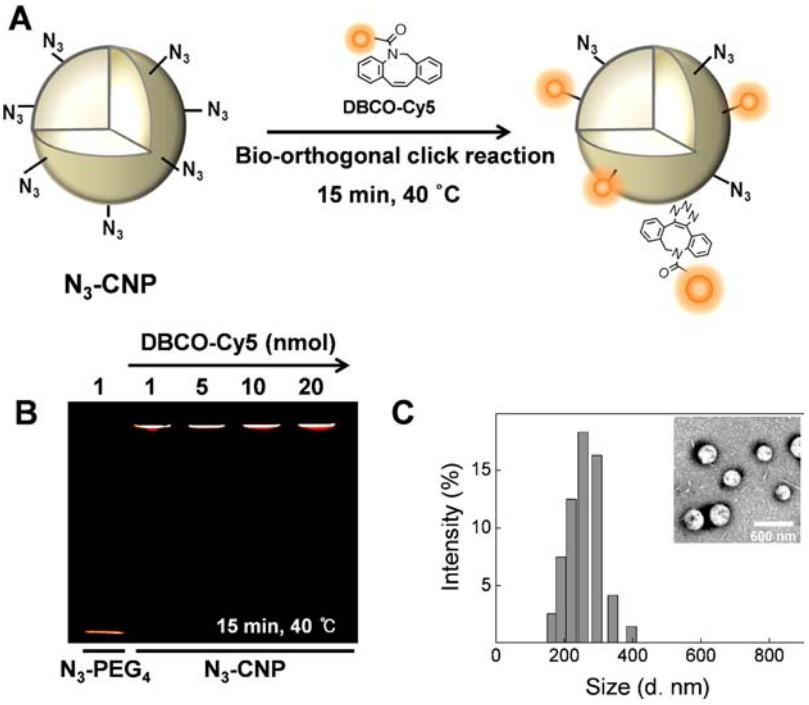

Figure 2. (A) Schematic illustration for labeling of signals onto azide-functionalized CNP via bio-orthogonal click chemistry. (B) SDS-PAGE analysis (40 °C, 15 min) for analysis of click reaction between CNP-N_3 and DBCO-Cy5. (C) Diameter distribution of Cy5-CNPs measured by dynamic light scattering (DLS) and transmission electron microscopy (TEM) images of CNP-N_3 (scale bar = 600 nm).

RESULTS

Preparation of Azide-Functionalized CNPs. The dual PET/optical probes based on CNPs were prepared by introduction of the ^{64}Cu-radiolabeled DOTA complex and the activatable MMP-probe onto the azide-functionalized CNPs via copper-free click chemistry (Figure 1). The ^{64}Cu-radiolabeled DOTA were used as imaging agent for PET, and the activatable MMP-probe was used as optical imaging agent to detect MMPs; the quenched NIR fluorescence by the quencher (BHQ-3) is activatable with specific cleavage of target MMPs.[26]

To prepare the azide-functionalized CNPs (CNP-N_3), the glycol chitosan (GC) polymers (M_w: 250 kDa) were conjugated with 23 wt % of hydrophobic 5β-cholanic acid (CA) and 5 wt % of the N_3-PEG_4. In a previous study, the formation of the amide linkage between N_3-PEG_4 and GC-CA was confirmed by the characteristic peaks for the azide (N_3) appearing at approximately 2110 cm^{-1} in FT-IR spectra.[28] Under optimal conditions, the contents of azide in the CNP-N_3 were 47 as determined by a colloidal titration method.[32]

The dibenzyl cyclooctyne (DBCO) was used as the specific functional group to conjugate with the azide groups of CNPs (Figure 1). To verify the interaction between CNP-N_3 with the DBCO via copper-free click chemistry, fluorescent dye conjugated DBCO derivative (DBCO-Cy5, (λ_{abs} 653 nm; λ_{em} 674 nm)) was used to monitor the extent of the click reaction by fluorescence under SDS-PAGE analysis (Figure 2). The CNP-N_3 (400 μg) was incubated with various amounts of DBCO-Cy5 at 40 °C for 15 min. The Cy5-labeled CNP-N_3 remained at the origin of the 5% stacking gel. In contrast, linear PEG_4-N_3 migrated from the origin to the bottom (Figure 2B). In addition, the fluorescent intensities of Cy5-labeled CNP-N_3 were increased up to 20 nmol of DBCO. This indicates that CNP-N_3 can perfectly conjugate with 20 nmol of DBCO within 15 min. The average size of the Cy5-labeled CNP-N_3 was 270 nm. Transmission electron microscopy (TEM) image also showed that Cy5-labeled CNP-N_3 was spherical in shape with uniform size distribution (Figure 2C).

Conjugation with Activatable MMP-Specific Peptide Probe-DBCO and ^{64}Cu-DOTA-Lys-PEG_4-DBCO in CNP-N_3. Activatable MMP-specific peptide probe (AMP) with DBCO group (AMP-DBCO) was synthesized by standard solid-phase Fmoc peptide chemistry as previously described with slight modification.[6] AMP-DBCO is composed of MMP-specific peptide, NIRF dye (Cy5.5), dark quencher (BHQ-3), and DBCO (Figure S1A). The conjugation of DBCO into AMP (AMP-DBCO) was monitored by HPLC (Figure S1B). The HPLC profiles of the reaction mixture after conjugating the DBCO to AMP showed one main peak, and the peak was matched with the reference peak of the MMP peptide probe. After conjugation of AMP-DBCO into CNP-N_3 (AMP-CNPs), the specificity of the AMP-CNPs was confirmed by MMP-2, 3, 7, 9, 13, and MMP-2/inhibitor in vitro. During 1 h incubation at 37 °C, significant recovery of the fluorescence signals occurred with MMP-2, MMP-9, and MMP-13. In contrast, the fluorescence signal was inhibited in MMP-2/inhibitor (Figure 3B). When the AMP-CNPs were treated various concentrations of MMP-2 for 1 h at 37 °C, the fluorescent signals of probe were recovered with concentration of MMP-2 (Figure 3C).

After subsequent conjugation of AMP into CNP-N_3, AMP-CNPs were conjugated with ^{64}Cu using simple two steps (pre-radiolabeling and post-conjugation via bio-orthogonal click chemistry); DOTA-Lys-PEG_4-DBCO was first radiolabeled with ^{64}Cu to form the ^{64}Cu-DOTA-Lys-PEG_4-DBCO complex (step 1: pre-radiolabeling), followed by the conjugation of ^{64}Cu-DOTA-Lys-PEG_4-DBCO with AMP-CNPs was performed via copper-free click reaction (step 2: post-conjugation) under mild reaction conditions (30 min at 40 °C in aqueous solution). The radiolabeling of ^{64}Cu-DOTA-Lys-PEG_4-DBCO

dx.doi.org/10.1021/bc500020g | Bioconjugate Chem. 2014, 25, 601−610

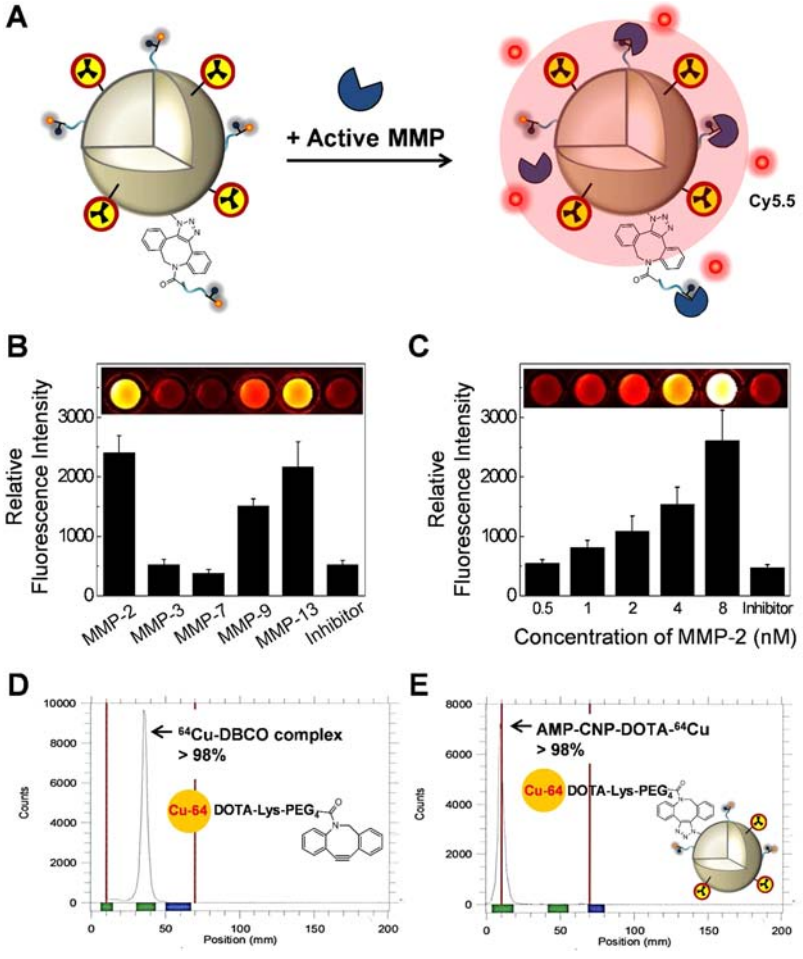

Figure 3. (A) Schematic illustration of MMP-sensitive probe; MMP-sensitive NS. Because of the efficient NIR fluorescence quenching ability of the quencher (BHQ-3) and self-quenching of the Cy5.5 dye itself, fluorogenic peptides that are chemically conjugated on the surface of nanoparticles are in the strongly multiquenched state. After cleavage of the substrate by MMPs, NIR fluorescence dyes are released from nanoparticles and fluoresce brightly. (B) Specificity and (C) sensitivity of MMP-sensitive probe. Radio-TLC analysis for radiolabeling yield (%) of (D) ^{64}Cu-DOTA-Lys-PEG$_4$-DBCO and (E) AMP-CNP-DOTA-^{64}Cu.

was achieved with high specific activity (18.5 GBq/μmol, 0.5 Ci/μmol) and the radiochemical purity (RCP) was consistently above 98% at standard radiolabeling condition, which can be used directly without further any purification (Figure 3D). After conjugation with ^{64}Cu-DOTA-Lys-PEG$_4$-DBCO via copper-free click reaction, the specific activity of radiolabeled AMP-CNPs-DOTA-^{64}Cu was 1 mCi/mg of nanoparticles with high radiochemical yield of above 98%, confirmed by following radio thin-layer chromatography (radio-TLC) (Figure 3E).

In Vivo NIRF and PET Multimodal Imaging Studies in Tumor-Bearing Mice. To validate the use of dual PET/activatable NIRF probe-labeled CNPs for tracking nanoparticles and imaging of tumor in vivo, whole-body NIRF and PET images were obtained in A549 tumor-bearing mice after intravenous injection of AMP-CNP-DOTA-^{64}Cu. Representative in vivo whole-body NIRF/PET images at selected time points were shown in Figure 4. An obvious NIRF signal was detected from the tumor region as early as 1 h postinjection, and NIRF signal was significantly increased and reached a plateau at 6 h (Figure 4A and B). Meanwhile, the NIRF signal in the tumor region was significantly reduced in the presence of MMP-inhibitor, confirming the specific cleavage of MMP probe. After 6 h postinjection, the NIRF signal intensity in the tumor region was about 3.8-fold higher than that of the inhibitor-treated group at 6 h postinjection (Figure 4B).

In vivo real-time biodistribution and tumor accumulation of AMP-CNP-DOTA-^{64}Cu were also demonstrated by whole-body PET imaging. Whole-body PET images are shown in Figure 4C, with the quantitative data obtained from ROI analysis of the PET images (Figure 4D). PET images revealed that the tumor accumulation of AMP-CNP-DOTA-^{64}Cu gradually increased with time, which reached a plateau at 24 h postinjection. However, at early time points (at 2 and 6 h post injection), tumor region was barely visible on the static PET images due to high radioactivity in abdomen. High radioactivity accumulation in the liver and the kidney was observed at all time points, but the retention of radioactivity in both organs was significantly reduced at 48 h postinjection. Meanwhile, blood circulation of AMP-CNP-DOTA-^{64}Cu assessed from the radioactivity in the cardiac pool was prominent at early time points, and gradually decreased as a function of time. As a result, the tumor uptake of AMP-CNP-DOTA-^{64}Cu was increased from 3.1 (% ID/g) at 2 h postinjection to 6.2 (% ID/g) at 24 h. Therefore, tumor region could definitely delineate from the surround tissues after 24 h postinjection.

dx.doi.org/10.1021/bc500020g | *Bioconjugate Chem.* 2014, 25, 601−610

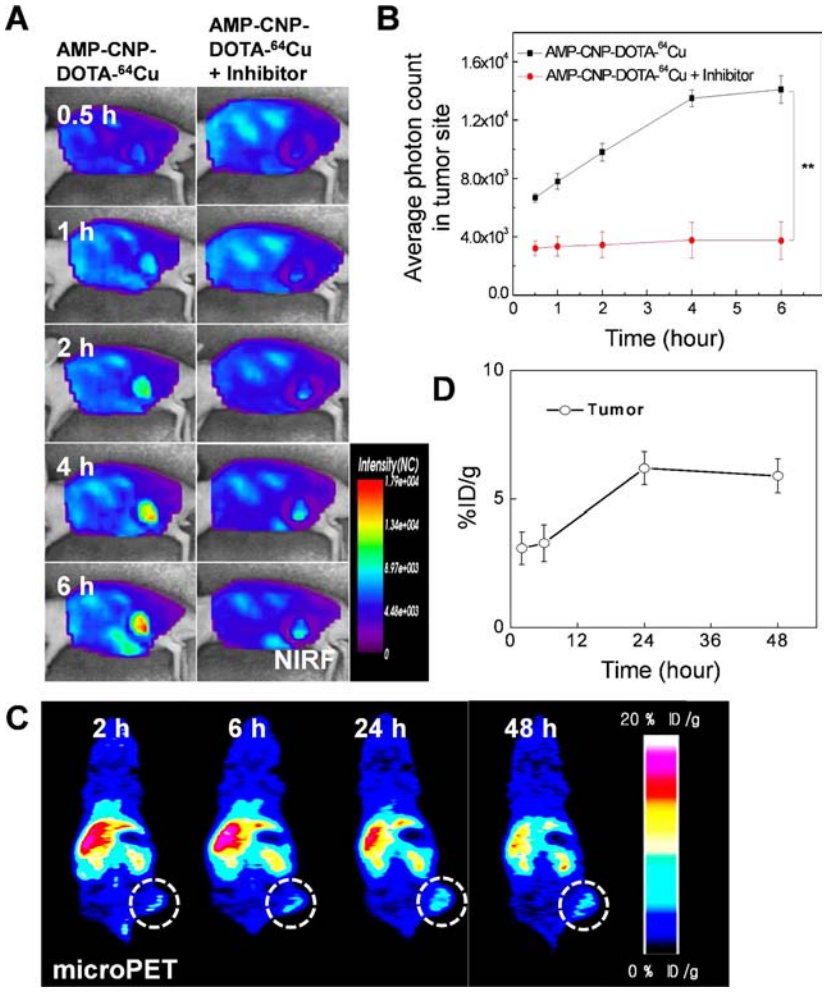

Figure 4. Time-dependent in vivo whole body (A) NIRF images and (C) micro PET images. White circles indicate the site of tumors. (B) and (D) Quantitative analysis of (A) and (C), respectively.

Ex Vivo NIRF Imaging and Biodistribution Studies. To confirm the observations of in vivo multimodal imaging, tumor and other major organs were excised, and their NIRF signal intensities and radioactivity were quantified through a NIRF imaging with Kodak Image Station and γ-counting (Figure 5). As expected, the highest NIRF signal intensity was observed in the tumor region, and the NIRF intensity was stronger than that of MMP-inhibitor-treated tumor, which was consistent with the whole body imaging. Interestingly, the NIRF intensity of the kidney in ex vivo imaging was much higher than that in the whole body NIRF image. The observed NIRF signal in kidney might be due to the excretion of cleaved fluorescent Cy5.5 dye-conjugated fragment, which was dissociated from the MMP probe after cleavage of MMP protease.

The in vivo biodistribution profile of CNP was also examined after the last PET scans at 48 h postinjection. Overall, the quantification results obtained from the biodistribution study are well correlated with the observation for major organs obtained from the PET image (Figure 5D). The tumor uptake of CNP was 5.60 ± 1.88%ID/g, thereby providing excellent tumor targeting. Liver, spleen, and kidney were organs of major AMP-CNP-DOTA-^{64}Cu accumulation. The blood still retained high radioactivity even at 48 h after injection.

DISCUSSION

There are high expectations for the use of imaging modality in diagnosis of cancer because clinical imaging can provide anatomic and physiological information without tissue biopsy process.[11,20,36,37] In addition, recently developed imaging technologies are capable of quantitating a variety of markers in the development of cancer.[7,38,39] Therefore, the combination of two imaging modalities may overcome weakness and enhance strengths of the single imaging modality. In this study, we developed a PET/optical activatable imaging probe based on glycol chitosan nanoparticles to overcome limitations of PET imaging. Chemically labeled activatable probes with MMP activatable peptide and ^{64}Cu showed high specificity and sensitivity in tumor-bearing mice.

This probe for dual imaging modality (PET/optical imaging) presents several advantages. First, azide functionalized CNPs were readily labeled with signals (MMP sensitive peptide and ^{64}Cu) via bio-orthogonal click chemistry. An ideal methodology to label signals on particles is composed of aqueous-based orthogonal chemistry that is free of additives and is achieved in a simple one-step reaction. In this study, we induced a facile method to label signals based on bio-orthogonal click chemistry. The bio-orthogonal click chemistry is a highly selective cycloaddition between an azide and strained cyclo-octyne derivative alkyne that is greatly accelerated in water.[40,41]

dx.doi.org/10.1021/bc500020g | Bioconjugate Chem. 2014, 25, 601−610

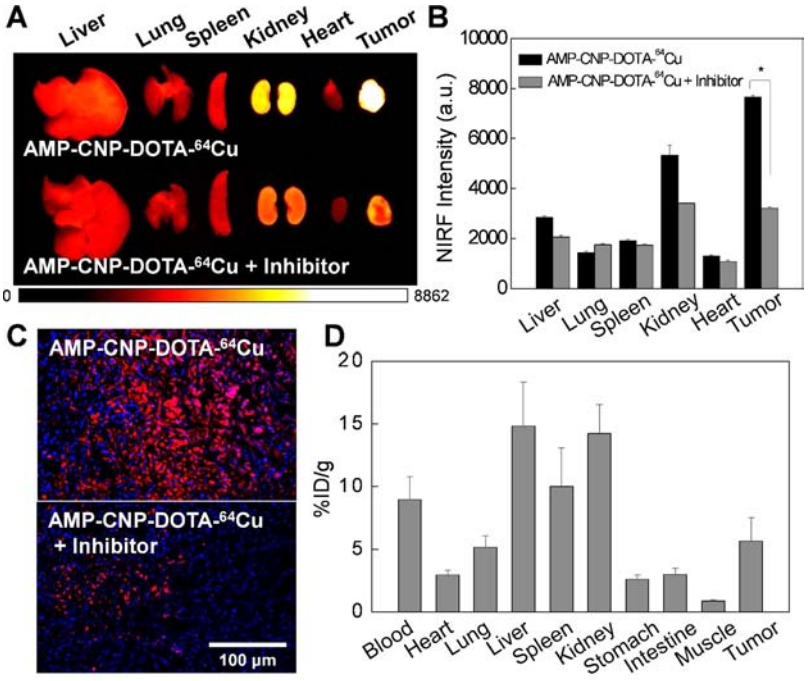

Figure 5. (A) Representative ex vivo fluorescence images of dissected organs from A549 tumor-bearing mice at 6 h. (B) Quantitative analysis of (A). (C) Fluorescence images of tumor tissues after intravenous injection of AMP-CNPs-DOTA-^{64}Cu. (D) Biodistribution of AMP-CNPs-DOTA-^{64}Cu in A549 tumor-bearing mice at 48 h after postinjection. Data are presented as percentage injected dose per gram (%ID/g).

In addition, this reaction is free from side reactions and byproduct.[42] Previous publications have reported that radiolabeling method under mild condition such as pH and temperature showed low labeling efficiency. In addition, these methods need the removal process of additives used for the chelation and purification step to reach high radiochemical purity.[28] Thus, it would be useful to label signals on particles for imaging probe.

Second, our probe for multimodal imaging can provide not only the quantitative information of tumor-targeting efficacy, but also the biological characteristics of cancer to select optimal cancer treatment planning. We developed an MMP-sensitive imaging nanoprobe based on CNPs for visualization of the activity of MMPs in cancer. When the MMP-sensitive imaging probe is exposed to the specific MMPs, the NIR-dye peptide is separated from quencher due to specific substrate recognition by the MMPs. The intensity of fluorescence then significantly increases.[26] MMPs are known to play critical roles in tumor progression and metastasis;[29,30] thus, overexpression of MMP activity is often found in tumor sites.[43,44] Previous publications have reported that the expression of MMPs is elevated in some tumors and accelerates tumor aggressiveness and metastasis.[45,46] Indeed, in our comparative study, the expression of MMP in various cancer cell lines (MCF-7, MDA-MB-231, and A549) showed different intensities (Figure S2C); compared to MCF-7, A549 expressed a high level of MMP (1.23-fold). In addition, wound healing assay results showed A549 has a 4.31-fold greater migration capacity as compared to MCF-7 (Figure S2A and B). This result may have been due to the different amounts of secreted bioactive MMPs, as the level of bioactive MMPs secreted by MCF-7 may have been insufficient to induce the active migration. Therefore, the detection of MMP activity in cancer provides important information for diagnosis, optimal cancer treatment planning, and therapeutic monitoring.

Considerable attention should be paid to the multimodal imaging approach that combines more than two imaging methods to provide complementary functional information.[8] In contrast, little attention has been given to PET/optical multimodal imaging due to the similar detection sensitivity of two imaging systems. However, this study demonstrated advantages of dual PET/optical imaging. The dual PET/optical multimodal imaging provided not only quantitative accuracy of imaging probes in tumor site, but also specific information on biological cancer microenvironment for optimal cancer treatment planning. Thus, these findings should benefit the clinical application of PET/optical multimodal imaging to provide accurate diagnosis of cancer and optimal treatment planning.

■ CONCLUSIONS

The data presented here demonstrate the sensitivity and quantitative capability of dual PET/optical probes based on CNPs. In this study, we have prepared activatable MMP peptide conjugated and radiolabeled CNPs with high specific activity via bio-orthogonal click chemistry. The stable triazole linker between the azide on the CNPs and DBCO makes it possible to label nanoparticles with ^{64}Cu and activatable MMP peptide efficiently and with high labeling yield. In addition, the highest MMP signal intensity and the tumor accumulation of AMP-CNP-DOTA-^{64}Cu was observed at the tumor region in tumor-bearing mice by optical system and PET, respectively. This technique should prove useful for accurate diagnosis of cancer and optimal treatment planning.

■ EXPERIMENTAL PROCEDURES

Materials. Glycol chitosan (M_w = 250 kDa; degree of deacetylation = 82.7%) was purchased from Sigma-Aldrich (St. Louis, MO, USA), purified by filtration, and dialyzed against deionized distilled water. 5β-cholanic acid, *N*-hydroxysuccinimide (NHS), *N*-hydroxysulfosuccinimide (sulfo-NHS; 98%), 1-

dx.doi.org/10.1021/bc500020g | *Bioconjugate Chem.* 2014, 25, 601−610

ethyl-3-(3-dimethylaminopropyl)-carbodiimide hydrochloride (EDC), *N*-methyl morpholine (NMM), 4-dimethylaminopyridine (DMAP), trifluoroacetic acid (TFA), and anhydrous dimethylformamide (DMF) were purchased from Sigma-Aldrich (St. Louis, MO, USA). Azide-PEG_4-NHS ester (N_3-PEG_4-NHS), dibenzylcyclooctyne-PEG_4-NHS ester (DBCO-PEG_4-NHS), DBCO-PEG_4-NH_2, and DBCO-Cy5 were purchased from Click Chemistry Tools (Scottsdale, AZ, USA). Cy5.5 mono *N*-hydroxysuccinamide ester (Cy5.5-NHS), black hole quencher-3 (BHQ-3), and protected matrix metalloproteinase (MMP) substrate (Gly-Pro-Leu-Gly-Val-Arg-Gly-Lys-Gly-Gly) were obtained from GE Healthcare (Piscataway, NJ, USA), Biosearch Technologies (Novato, CA, USA), and Peptron Inc. (Daejeon, Korea), respectively. MMP-2, MMP-3, MMP-7, MMP-9, MMP-13 enzyme, and MMP-2 inhibitor were bought from R&D Systems (Minneapolis, MN, USA). 1,4,7,10-Tetraazacyclododecane-1,4,7-tris(*t*-butyl acetate)-10-acetic acid [DOTA-tris(*t*-Bu) ester], and Fmoc-Lys(Dde)-OH were purchased from Macrocyclics (Dallas, TX, USA), and Anaspec (Frenont, CA, USA), respectively. $^{64}CuCl_2$ was obtained from a cyclotron at Korea Institute of Radiological and Medical Science (KIRAMS) (Seoul, Korea). All other chemicals were of analytical grade and used without any purification.

Synthesis of Azide-Functionalized CNPs (N_3-CNPs). Self-assembled glycol chitosan nanoparticles (CNPs) were prepared by chemically conjugating hydrophobic 5β-cholanic acid to the primary amine groups of glycol chitosan polymers as previously reported.[31] Briefly, to activate carboxylic acid group of 5β-cholanic acid with NHS, 5β-cholanic acid (150 mg, 400 μmol) was dissolved in 60 mL methanol and mixed with EDC (120 mg, 600 μmol, 1.5 equiv of 5β-cholanic acid), and NHS (72 mg, 600 μmol, 1.5 equiv of 5β-cholanic acid). Then, glycol chitosan (500 mg, 2 μmol) was dissolved in deionized distilled water/methanol mixture (1:1 v/v, 60 mL) and added to the methanol solution containing NHS-activated 5β-cholanic acid. The resulting solution was stirred overnight at room temperature, and then dialyzed for 3 days in deionized distilled water/methanol (1:3 v/v) using a cellulose membrane (MWCO 12−14000, Spectrum Laboratories, Laguna Hills, CA, USA). The solution was further dialyzed for 1 day in deionized distilled water and lyophilized to give glycol chitosan-5β-cholanic acid conjugates. The degree of substitution (DS), defined as the number of 5β-cholanic acid per one glycol chitosan polymer, was determined using a colloidal titration method as previously described.[32] The final conjugates had 150 ± 4.5 molecules of 5β-cholanic acids per one glycol chitosan polymer.

To prepare azide (N_3)-functionalized CNPs (N_3-CNPs), N_3-PEG_4-NHS was chemically conjugated to the glycol chitosan-5β-cholanic acid conjugates using the similar amide bond formation. Briefly, N_3-PEG_4-NHS (3.7 mg, 9.5 μmol) was dissolved in 500 μL of DMSO and added dropwise to the glycol chitosan-5β-cholanic acid conjugate solution (20 mg, 4 mL) in DMSO. The reaction mixture was stirred overnight at room temperature, dialyzed against deionized distilled water using a cellulose membrane (MWCO 12−14000) for 2 days, and lyophilized to obtain white powder. Formation of the amide linkage between N_3-PEG_4 and glycol chitosan-5β-cholanic acid conjugates was confirmed by the characteristic peaks of the azide (N_3) in Fourier transform infrared (FT-IR) spectra as previously reported.[28] The DS of N_3-PEG_4 per molecule of glycol chitosan−5β-cholanic acid conjugates was determined using a colloidal titration method. The resulting samples were dispersed in deionized distilled water or PBS buffer (pH 7.4) by sonication to produce nanosized N_3-CNPs. The sizes and morphological shapes of N_3-CNPs were measured using a Zetasizer Nano ZS (Malvern Instruments, Worcestershire, UK) and transmission electron microscopy (TEM). The copper-free click reaction between N_3-CNPs and DBCO derivatives was evaluated by an SDS-polyacrylamide gel electrophoresis (PAGE) assay. N_3-CNPs (200 μL, 2 mg/mL) were reacted with various mole ratios of DBCO-Cy5 (1−20 nmol) for 15 min at 40 °C. After incubation, the resulting Cy5 labeled CNPs (Cy5-CNPs) were loaded onto 8% SDS-PAGE gel for electrophoresis. Fluorescence images of the gel were obtained with a 12-bit CCD (Kodak Image Station 4000 MM, New Haven, CT, USA) equipped with a special C-mount lens and a near-infrared emission filter (600−700 nm; Omega Optical, Brattleboro, VT, USA).

Synthesis of Cy5.5 and BHQ-3 Conjugated MMP Substrate Peptide (Activatable MMP Probe). The MMP probe was prepared by conjugating near-infrared fluorescence (NIRF) dye, Cy5.5 (ex/em; 675/695 nm) and BHQ-3 (abs. 650 nm) to MMP substrate peptide as previously described.[6] Briefly, MMP substrate peptides (Gly-Pro-Leu-**Gly-Val**-Arg-(pbf)-Gly-Lys(boc)-Gly-Gly; the cleavage site is between Gly and Val[33]) were synthesized using standard solid-phase Fmoc peptide chemistry. Then, Cy5.5-NHS (8.4 μmol) was coupled to the N-terminus of the MMP substrate peptides (4.0 μmol) in DMF (200 μL) containing DMAP (2.5 μmol) and NMM (52 μmol) at room temperature under stirring for 4 h in the dark. The Cy5.5 conjugated MMP substrate peptides were precipitated by adding diethyl ether. The precipitates were washed with diethyl ether and dried in vacuum chamber. After removal of side chain protecting groups, Cy5.5-MMP substrate peptides were purified through analytical reversed-phase high performance liquid chromatography (RP-HPLC; Agilent 1200 series, Agilent Technologies, Palo Alto, CA, USA). Then, the BHQ-3 (0.9 μmol) was coupled to the primary amine of the lysine of the Cy5.5-MMP substrate peptides (0.9 μmol) in DMF (30 μL) containing DMAP (1.0 μmol) and NMM (9.7 μmol) at room temperature in the dark under stirring overnight. The products were also purified by RP-HPLC.

Synthesis of DBCO Conjugated Activatable MMP Probe (AMP-DBCO). Activatable MMP probe (AMP) (1.0 mg), EDC (0.6 mg), and sulfo-NHS (0.8 mg) were dissolved in 100 μL DMSO/200 μL PBS (pH = 6.0) and stirred vigorously for 15 min. After stirring, the solutions were added to DBCO-PEG_4-NH_2 (0.3 mg, 1.0 mL in PBS (pH = 6.0)) and kept under stirring overnight in the dark. The products were also purified and analyzed by RP-HPLC: 5% to 95% acetonitrile containing 0.1% TFA versus deionized distilled water containing 0.1% TFA over 25 min at a flow rate of 1.0 mL/min.

Synthesis of DOTA-Lys-PEG_4-DBCO. DOTA-Lys-PEG4-DBCO was synthesized using standard solid-phase Fmoc peptide chemistry in Peptron Inc. (Daejeon, Korea) as previously reported.[28] Briefly, resin conjugated Fmoc-Lys-(Dde)-OH was used as a solid support of the reaction. After Fmoc group of Fmoc-Lys(Dde)-O-Resin was removed and followed by Boc protection, Dde group was removed with 2% hydrazine in DMF. DOTA-tris(*t*-Bu ester) was then coupled with (Boc)-Lys(H)-O-Resin. After coupling, the product was cleaved from the support by treatment with 95% TFA containing 2.5% triisopropylsilane (TIS) and 2.5% deionized distilled water (TFA:TIS:DDW = 9.5:2.5:2.5). Then, DBCO-PEG_4-NHS was coupled with DOTA-Lys to produce DOTA-

dx.doi.org/10.1021/bc500020g | *Bioconjugate Chem.* 2014, 25, 601−610

Lys-PEG_4-DBCO. The product was purified and analyzed by Shimadzu HPLC.

Conjugation of CNPs with Activatable MMP Probe (AMP-CNPs). Conjugation of N_3-CNPs with AMP-DBCO was accomplished with the simple copper-free click reaction. Briefly, N_3-CNPs (1 mL, 2 mg/mL) were incubated with AMP-DBCO (50 nmol) for 15 min at 40 °C in aqueous condition to prepare AMP-CNPs. The sizes and morphological shapes of AMP-CNPs were measured using a Zetasizer Nano ZS (Malvern Instruments, Worcestershire, UK) and TEM.

In Vitro MMP Activity Test of AMP-CNPs. NIR fluorescence (NIRF) recovery of AMP-CNPs was examined in terms of MMP enzyme specificity and concentration of MMP enzyme. MMP enzymes (MMP-2, 3, 7, 9, or 13) were activated by incubation for 1 h at 37 °C with 2.5 nM of *p*-aminophenyl mercuric acid in the TCNB buffer. The same amount of AMP-CNPs was added to MMP enzyme solution and incubated additionally for 1 h at 37 °C. The intensity of recovered fluorescence, which depended on the concentration of MMP enzymes, was monitored by Kodak Image Station 4000 MM equipped with filter systems for Cy5.5.

In Vitro Cell Migration Test. MCF-7, MDA-MB-231 (Human breast adenocarcinoma), and A549 (Human lung adenocarcinoma) cells were purchased from ATCC (Manassas, VA, USA), maintained in RPMI1640 (Welgene, Daegu, Korea) containing 10% fetal bovine serum (FBS; Welgene, Daegu, Korea) and 100 μg/mL streptomycin and 100 U/mL penicillin (Welgene, Daegu, Korea) in a humidified 5% CO_2 atmosphere at 37 °C. MCF-7, MDA-MB-231, and A549 cells were seeded onto 100 × 20 mm^2 cell culture plates at a density of 2×10^6 cells per plate and grown to reach 70−80% confluence. Then, the cell monolayer was wounded with a p200 tip and the plates were washed and incubated at 37 °C in growth media for 24 h. Cell migration images were observed with a light microscope (BX51, Olympus, Tokyo, Japan) and photographed on a digital camera photomicroscope (DP71, Olympus, Tokyo, Japan). The rate of migration was calculated by measuring the distance moved toward the center of the wound in 24 h.

In Vitro MMP Activity Test of Various Cancer Cell Lines. MCF-7, MDA-MB-231, and A549 cells were seeded onto 96-well flat-bottomed plates at a density of 1×10^4 cells per well and allowed to adhere for 20 h. The cells were exposed to AMP-CNPs (final concentration: 0.5 mg/mL) in cell culture media for 1 h. The 96-well plate was visualized with Kodak Image Station 4000 MM equipped with filter systems for Cy5.5.

Pre-Radiolabeling: Preparation of Radiolabeled ^{64}Cu-DOTA-Lys-PEG_4-DBCO. The DOTA-Lys-PEG_4-DBCO was dissolved in deionized distilled water to give a concentration of 10^{-3} M (10^{-6} mol/mL). Cyclotron-produced $^{64}CuCl_2$ solutions (stock solution: 5 mCi (185 MBq) in 50 μL of 0.01 N HCl) were mixed with the DOTA-Lys-PEG_4-DBCO (10^{-9} mol) in 100 μL of 50 mM sodium acetate buffer (pH 5.5), resulting in a final concentration of 5 mCi/ml (0.5 mCi (18.5 MBq)/10^{-9} mol of DOTA-Lys-PEG_4-DBCO in 100 μL), and the reaction was allowed to stand for 30 min at 40 °C. The reaction solutions were analyzed by radio thin-layer chromatography (radio-TLC) on aluminum-backed silica gel sheets developed with 0.1 M citrate and 10% ammonium acetate/methanol (1/1, v/v) as a mobile phase to check the radiolabeled complex. Radioactivity on radio-TLC was scanned using a Bioscan System 200 Imaging Scanner (Washington, DC, USA).

Post-Conjugation: Conjugation of N_3-CNPs with AMP-DBCO and ^{64}Cu-DOTA-Lys-PEG_4-DBCO via Copper-Free Click Chemistry (AMP-CNPs-DOTA-^{64}Cu). Dual labeling of N_3-CNPs with AMP-DBCO and ^{64}Cu-DOTA-Lys-PEG_4-DBCO was accomplished with the simple copper-free click reaction. Briefly, N_3-CNPs (2 mg/mL) were incubated with AMP-DBCO (50 nmol) and ^{64}Cu-DOTA-Lys-PEG_4-DBCO (0.5 mCi (18.5 MBq)/10^{-9} mol of DOTA-Lys-PEG_4-DBCO in 100 μL) for 30 min at 40 °C in aqueous condition to prepare dual-labeled nanoparticles (AMP-CNPs-DOTA-^{64}Cu). DOTA precursor was first chelated with ^{64}Cu followed by conjugated onto N_3-CNPs using bio-orthogonal click chemistry. After the reaction, the efficiency of the copper-free click reaction and the radiochemical yield of radiolabeled AMP-CNPs-DOTA-^{64}Cu were determined by radio-TLC as described above.

In Vivo and ex Vivo NIRF Imaging. All experiments with live animals were performed in compliance with the relevant laws and institutional guidelines of Korea Institute of Science and Technology (KIST), and institutional committees approved the experiments. For the evaluation of in vivo and ex vivo experiments with AMP-CNPs-DOTA-^{64}Cu, A549 tumor cells (1.0×10^7 cells) were injected subcutaneously on flanks of 4-week-old male athymic nude mice (20 g, Institute of Medical Science, Tokyo, Japan). When the tumor reached about 100 mm^2, AMP-CNPs-DOTA-^{64}Cu (10 mg/kg) were injected into the tail vein of the A549 tumor-bearing mice. For inhibition experiment, MMP inhibitor (100 μg/mL) was intratumorally injected into the A549 tumors, 30 min prior to injection of the AMP-CNP-DOTA-^{64}Cu. The NIRF tomographic images were obtained by eXplore Optix system (ART Advanced Research Technologies Inc., Montreal, Canada). Laser power and count time settings were optimized at 25 μW and 0.3 s per point. Excitation and emission spots were raster-scanned in 1 mm steps over the selected region of interest to generate emission wavelength scans. A 670 nm pulsed laser diode was applied to excite Cy5.5 molecules. NIRF emission at 700 nm was collected and detected with a fast photomultiplier tube (Hamamatsu, Japan) and a time-correlated single photon counting system (Becker and Hickl GmbH, Berlin, Germany).[34] The major organs and tumors (n = 3 per each group) were dissected from mice 6 h postinjection of AMP-CNPs-DOTA-^{64}Cu. NIRF images were obtained with Kodak Image Station 4000 MM equipped with filter systems for Cy5.5.

Histological Analysis. The dissected tumor tissues were embedded in optimum cutting temperature (OCT) compound (Sakura, Tokyo, Japan) and frozen in a deep freezer at −70 °C. Sections were cut on a cryostat (10 μm in thickness) and picked up on slides with poly-D-lysine, dried, protected from light. Fluorescence was observed (excitation: 673 nm, emission: 692 nm) using IX81-ZDC focus drift compensating microscope (Olympus, Tokyo, Japan).

microPET Imaging and Biodistribution Studies. All experiments with live animals were performed in compliance with the relevant laws and institutional guidelines of Samsung Medical Center, and institutional committees approved the experiments. For the in vivo microPET imaging, preparation of A549 tumor-bearing mice models and intravenous injection of AMP-CNPs-DOTA-^{64}Cu (0.3 mCi (111.1 MBq) of ^{64}Cu per 200 μg of CNPs, injection dose; 10 mg/kg of AMP-CNPs-DOTA-^{64}Cu) were performed by the same method. Mice were anesthetized with 1.5−2% isoflurane before being placed in the camera bed positioned prone. Static PET scans were acquired at 2, 6, 24, and 48 h post injection using the Inveon microPET/CT scanner, which has 10 cm transaxial and 12.7 cm axial field of view and operates exclusively in 3D mode (Siemens Medical

Solutions, Malvern, PA, USA).[35] The static microPET images were reconstructed using 3D-ordered subset expectation maximization. Then, the images were processed using Siemens Inveon Research Workplace 4.0 (IRW 4.0). For each scan, regions of interest (ROI) were drawn over tumors on whole-body axial images. All ROI values were decay corrected, and percent injected dose (%ID) and percent injected dose per gram of tumor (%ID/g of tumor) were measured by dividing the decay corrected ROI value for a given tumor by the injected dose activity with appropriate decay corrections. For biodistribution studies, AMP-CNPs-DOTA-^{64}Cu (1.1 MBq (30 μCi)/200 μL) were injected into the tail vein of the A549 tumor-bearing mice. After 48 h postinjection, the mice were sacrificed. Blood, muscle, tumor, and major organs (heart, lung, liver, spleen, kidney, stomach, and intestine) were subsequently dissected and counted in a Wallac 1470 Wizard automated gamma counter (PerkinElmer Life Sciences) to measure the radioactivity. Percent injected dose (%ID) and percent injected dose per gram of organ (%ID/g organ) were calculated from standard control activity with appropriate decay corrections. All groups consisted of four or five mice. All mean values are given as ±SD.

■ ASSOCIATED CONTENT

Supporting Information

Details of synthesis and wound healing assay. This material is available free of charge via the Internet at http://pubs.acs.org.

■ AUTHOR INFORMATION

Corresponding Authors

* Tel.: +82-2-3410-2630; Fax: +82-2-3410-2639; E-mail: khnm.lee@samsung.com.

*Tel.: +82-2-958-5916; Fax: +82-2-958-5909; E-mail: kim@kist.re.kr.

Author Contributions

Sangmin Lee and Sun-Woong Kang contributed equally to this work.

Notes

The authors declare no competing financial interest.

■ ACKNOWLEDGMENTS

This work was supported by the KIST intramural project (Translational Research Program), the Global Research Laboratory (GRL), the Fusion Technology Project (2010-50201), and M.D.-Ph.D. Program (2010-0019863).

■ REFERENCES

(1) Nikiforov, Y. E., and Nikiforova, M. N. (2011) Molecular genetics and diagnosis of thyroid cancer. *Nat. Rev. Endocrinol. 7*, 569−80.

(2) Momparler, R. L. (2003) Cancer epigenetics. *Oncogene 22*, 6479−83.

(3) Mariani-Costantini, R. (2013) Diagnosis: Breast cancer screening in rural African communities. *Nat. Rev. Clin. Oncol. 10*, 185−6.

(4) Chen, X., Ba, Y., Ma, L., Cai, X., Yin, Y., Wang, K., Guo, J., Zhang, Y., Chen, J., Guo, X., Li, Q., Li, X., Wang, W., Zhang, Y., Wang, J., Jiang, X., Xiang, Y., Xu, C., Zheng, P., Zhang, J., Li, R., Zhang, H., Shang, X., Gong, T., Ning, G., Wang, J., Zen, K., Zhang, J., and Zhang, C. Y. (2008) Characterization of microRNAs in serum: a novel class of biomarkers for diagnosis of cancer and other diseases. *Cell Res. 18*, 997−1006.

(5) Nam, T., Park, S., Lee, S. Y., Park, K., Choi, K., Song, I. C., Han, M. H., Leary, J. J., Yuk, S. A., Kwon, I. C., Kim, K., and Jeong, S. Y. (2010) Tumor targeting chitosan nanoparticles for dual-modality optical/MR cancer imaging. *Bioconjugate Chem. 21*, 578−82.

(6) Sun, I. C., Eun, D. K., Koo, H., Ko, C. Y., Kim, H. S., Yi, D. K., Choi, K., Kwon, I. C., Kim, K., and Ahn, C. H. (2011) Tumor-targeting gold particles for dual computed tomography/optical cancer imaging. *Angew. Chem. 50*, 9348−51.

(7) Willmann, J. K., van Bruggen, N., Dinkelborg, L. M., and Gambhir, S. S. (2008) Molecular imaging in drug development. *Nat. Rev. Drug Discovery 7*, 591−607.

(8) Lee, D. E., Koo, H., Sun, I. C., Ryu, J. H., Kim, K., and Kwon, I. C. (2012) Multifunctional nanoparticles for multimodal imaging and theragnosis. *Chem. Soc. Rev. 41*, 2656−72.

(9) Kryza, D., Taleb, J., Janier, M., Marmuse, L., Miladi, I., Bonazza, P., Louis, C., Perriat, P., Roux, S., Tillement, O., and Billotey, C. (2011) Biodistribution study of nanometric hybrid gadolinium oxide particles as a multimodal SPECT/MR/optical imaging and theragnostic agent. *Bioconjugate Chem. 22*, 1145−52.

(10) Roberts, P. J., Stinchcombe, T. E., Der, C. J., and Socinski, M. A. (2010) Personalized medicine in non-small-cell lung cancer: is KRAS a useful marker in selecting patients for epidermal growth factor receptor-targeted therapy? *J. Clin. Oncol. 28*, 4769−77.

(11) Ferrari, M. (2005) Cancer nanotechnology: opportunities and challenges. *Nat. Rev. Cancer 5*, 161−71.

(12) Pepe, M. S., Etzioni, R., Feng, Z., Potter, J. D., Thompson, M. L., Thornquist, M., Winget, M., and Yasui, Y. (2001) Phases of biomarker development for early detection of cancer. *J. Natl. Cancer Inst. 93*, 1054−61.

(13) Weissleder, R. (2006) Molecular imaging in cancer. *Science 312*, 1168−71.

(14) Quon, A., and Gambhir, S. S. (2005) FDG-PET and beyond: molecular breast cancer imaging. *J. Clin. Oncol. 23*, 1664−73.

(15) Gambhir, S. S. (2002) Molecular imaging of cancer with positron emission tomography. *Nat. Rev. Cancer 2*, 683−93.

(16) Liu, S. (2008) Bifunctional coupling agents for radiolabeling of biomolecules and target-specific delivery of metallic radionuclides. *Adv. Drug Delivery Rev. 60*, 1347−70.

(17) Hong, H., Zhang, Y., Sun, J., and Cai, W. (2009) Molecular imaging and therapy of cancer with radiolabeled nanoparticles. *Nano Today 4*, 399−413.

(18) Liu, Y., and Welch, M. J. (2012) Nanoparticles labeled with positron emitting nuclides: advantages, methods, and applications. *Bioconjugate Chem. 23*, 671−82.

(19) Cheng, Z., Al Zaki, A., Hui, J. Z., Muzykantov, V. R., and Tsourkas, A. (2012) Multifunctional nanoparticles: cost versus benefit of adding targeting and imaging capabilities. *Science 338*, 903−10.

(20) Koo, H., Huh, M. S., Ryu, J. H., Lee, D.-E., Sun, I.-C., Choi, K., Kim, K., and Kwon, I. C. (2011) Nanoprobes for biomedical imaging in living systems. *Nano Today 6*, 204−220.

(21) Liu, T. W., Macdonald, T. D., Jin, C. S., Gold, J. M., Bristow, R. G., Wilson, B. C., and Zheng, G. (2013) Inherently multimodal nanoparticle-driven tracking and real-time delineation of orthotopic prostate tumors and micrometastases. *ACS Nano 7*, 4221−32.

(22) Maeda, H., Wu, J., Sawa, T., Matsumura, Y., and Hori, K. (2000) Tumor vascular permeability and the EPR effect in macromolecular therapeutics: a review. *J. Controlled Release 65*, 271−84.

(23) Shi, M., Lu, J., and Shoichet, M. S. (2009) Organic nanoscale drug carriers coupled with ligands for targeted drug delivery in cancer. *J. Mater. Chem. 19*, 5485−5498.

(24) Lee, S., Choi, K. Y., Chung, H., Ryu, J. H., Lee, A., Koo, H., Youn, I. C., Park, J. H., Kim, I. S., Kim, S. Y., Chen, X., Jeong, S. Y., Kwon, I. C., Kim, K., and Choi, K. (2011) Real time, high resolution video imaging of apoptosis in single cells with a polymeric nanoprobe. *Bioconjugate Chem. 22*, 125−31.

(25) Ryu, J. H., Kim, S. A., Koo, H., Yhee, J. Y., Lee, A., Na, J. H., Youn, I., Choi, K., Kwon, I. C., Kim, B.-S., and Kim, K. (2011) Cathepsin B-sensitive nanoprobe for in vivo tumor diagnosis. *J. Mater. Chem. 21*, 17631−17634.

(26) Lee, S., Ryu, J. H., Park, K., Lee, A., Lee, S. Y., Youn, I. C., Ahn, C. H., Yoon, S. M., Myung, S. J., Moon, D. H., Chen, X., Choi, K., Kwon, I. C., and Kim, K. (2009) Polymeric nanoparticle-based

activatable near-infrared nanosensor for protease determination in vivo. *Nano Lett. 9*, 4412−6.
(27) Ryu, J. H., Na, J. H., Ko, H. K., You, D. G., Park, S., Jun, E., Yeom, H. J., Seo, D. H., Park, J. H., Jeong, S. Y., Kim, I. S., Kim, B. S., Kwon, I. C., Choi, K., and Kim, K. (2014) Non-invasive optical imaging of cathepsin B with activatable fluorogenic nanoprobes in various metastatic models. *Biomaterials 35*, 2302−11.
(28) Lee, D. E., Na, J. H., Lee, S., Kang, C. M., Kim, H. N., Han, S. J., Kim, H., Choe, Y. S., Jung, K. H., Lee, K. C., Choi, K., Kwon, I. C., Jeong, S. Y., Lee, K. H., and Kim, K. (2013) Facile method to radiolabel glycol chitosan nanoparticles with (64)Cu via copper-free click chemistry for MicroPET imaging. *Mol. Pharmaceutics 10*, 2190−8.
(29) Egeblad, M., and Werb, Z. (2002) New functions for the matrix metalloproteinases in cancer progression. *Nat. Rev. Cancer 2*, 161−74.
(30) Coussens, L. M., and Werb, Z. (2002) Inflammation and cancer. *Nature 420*, 860−7.
(31) Na, J. H., Lee, S. Y., Lee, S., Koo, H., Min, K. H., Jeong, S. Y., Yuk, S. H., Kim, K., and Kwon, I. C. (2012) Effect of the stability and deformability of self-assembled glycol chitosan nanoparticles on tumor-targeting efficiency. *J. Controlled Release 163*, 2−9.
(32) Kwon, S., Park, J. H., Chung, H., Kwon, I. C., Jeong, S. Y., and Kim, I.-S. (2003) Physicochemical characteristics of self-assembled nanoparticles based on glycol chitosan bearing 5*B*-cholanic acid. *Langmuir 19*, 10188−10193.
(33) Bremer, C., Tung, C. H., and Weissleder, R. (2001) In vivo molecular target assessment of matrix metalloproteinase inhibition. *Nat. Med. 7*, 743−8.
(34) Na, J. H., Koo, H., Lee, S., Min, K. H., Park, K., Yoo, H., Lee, S. H., Park, J. H., Kwon, I. C., Jeong, S. Y., and Kim, K. (2011) Real-time and non-invasive optical imaging of tumor-targeting glycol chitosan nanoparticles in various tumor models. *Biomaterials 32*, 5252−61.
(35) Lee, I., Yoon, K. Y., Kang, C. M., Lin, X., Chen, X., Kim, J. Y., Kim, S. M., Ryu, E. K., and Choe, Y. S. (2012) Evaluation of the angiogenesis inhibitor KR-31831 in SKOV-3 tumor-bearing mice using (64)Cu-DOTA-VEGF(121) and microPET. *Nucl. Med. Biol. 39*, 840−6.
(36) Nahrendorf, M., Keliher, E., Marinelli, B., Waterman, P., Feruglio, P. F., Fexon, L., Pivovarov, M., Swirski, F. K., Pittet, M. J., Vinegoni, C., and Weissleder, R. (2010) Hybrid PET-optical imaging using targeted probes. *Proc. Natl. Acad. Sci. U.S.A. 107*, 7910−5.
(37) Kelkar, S. S., and Reineke, T. M. (2011) Theranostics: combining imaging and therapy. *Bioconjugate Chem. 22*, 1879−903.
(38) Josephson, L., Kircher, M. F., Mahmood, U., Tang, Y., and Weissleder, R. (2002) Near-infrared fluorescent nanoparticles as combined MR/optical imaging probes. *Bioconjugate Chem. 13*, 554−60.
(39) Janib, S. M., Moses, A. S., and MacKay, J. A. (2010) Imaging and drug delivery using theranostic nanoparticles. *Adv. Drug Delivery Rev. 62*, 1052−63.
(40) Boyce, M., and Bertozzi, C. R. (2011) Bringing chemistry to life. *Nat. Methods 8*, 638−42.
(41) Koo, H., Lee, S., Na, J. H., Kim, S. H., Hahn, S. K., Choi, K., Kwon, I. C., Jeong, S. Y., and Kim, K. (2012) Bioorthogonal copper-free click chemistry in vivo for tumor-targeted delivery of nanoparticles. *Angew. Chem. 51*, 11836−40.
(42) Jewett, J. C., and Bertozzi, C. R. (2010) Cu-free click cycloaddition reactions in chemical biology. *Chem. Soc. Rev. 39*, 1272−9.
(43) Zucker, S., and Vacirca, J. (2004) Role of matrix metalloproteinases (MMPs) in colorectal cancer. *Cancer Metastasis Reviews 23*, 101−17.
(44) Coussens, L. M., Fingleton, B., and Matrisian, L. M. (2002) Matrix metalloproteinase inhibitors and cancer: trials and tribulations. *Science 295*, 2387−92.
(45) Gupta, G. P., and Massague, J. (2006) Cancer metastasis: building a framework. *Cell 127*, 679−95.
(46) Vihinen, P., Ala-aho, R., and Kahari, V. M. (2005) Matrix metalloproteinases as therapeutic targets in cancer. *Curr. Cancer Drug Targets 5*, 203−20.